

## $\Lambda$ Production and Flow in Au+Au Collisions at 11.5A GeV/c

J. Barrette<sup>5</sup>, R. Bellwied<sup>9</sup>, S. Bennett<sup>9</sup>, R. Bersch<sup>7</sup>, P. Braun-Munzinger<sup>2</sup>, W. C. Chang<sup>7</sup>,  
 W. E. Cleland<sup>6</sup>, M. Clemen<sup>6</sup>, J. Cole<sup>4</sup>, T. M. Cormier<sup>9</sup>, Y. Dai<sup>5</sup>, G. David<sup>1</sup>, J. Dee<sup>7</sup>,  
 O. Dietzsch<sup>8</sup>, M. Drigert<sup>4</sup>, K. Filimonov<sup>3</sup>, S. C. Johnson<sup>7</sup>, J. R. Hall<sup>9</sup>, T. K. Hemmick<sup>7</sup>,  
 N. Herrmann<sup>2</sup>, B. Hong<sup>2</sup>, Y. Kwon<sup>7</sup>, R. Lacasse<sup>5</sup>, Q. Li<sup>9</sup>, T. W. Ludlam<sup>1</sup>, S. K. Mark<sup>5</sup>,  
 R. Matheus<sup>9</sup>, S. McCorkle<sup>1</sup>, J. T. Murgatroyd<sup>9</sup>, D. Miśkowiec<sup>2</sup>, E. O'Brien<sup>1</sup>, S. Panitkin<sup>7</sup>,  
 V. Pantuev<sup>7</sup>, P. Paul<sup>7</sup>, T. Piazza<sup>7</sup>, M. Pollack<sup>7</sup>, C. Pruneau<sup>9</sup>, Y. J. Qi<sup>5</sup>, M. N. Rao<sup>7</sup>,  
 E. Reber<sup>4</sup>, M. Rosati<sup>5</sup>, N. C. daSilva<sup>8</sup>, S. Sedykh<sup>7</sup>, U. Sonnadara<sup>6</sup>, J. Stachel<sup>3</sup>,  
 E. M. Takagui<sup>8</sup>, V. Topor Pop<sup>5</sup>, M. Trzaska<sup>7</sup>, S. Voloshin<sup>6</sup>, T. B. Vongpaseuth<sup>7</sup>,  
 G. Wang<sup>5</sup>, J. P. Wessels<sup>3</sup>, C. L. Woody<sup>1</sup>, N. Xu<sup>7</sup>, Y. Zhang<sup>7</sup>, C. Zou<sup>7</sup>

(E877 Collaboration)

<sup>1</sup> *Brookhaven National Laboratory, Upton, NY 11973*

<sup>2</sup> *Gesellschaft für Schwerionenforschung, 64291 Darmstadt, Germany*

<sup>3</sup> *Universität Heidelberg, 69120 Heidelberg, Germany*

<sup>4</sup> *Idaho National Engineering Laboratory, Idaho Falls, ID 83402*

<sup>5</sup> *McGill University, Montreal, Canada*

<sup>6</sup> *University of Pittsburgh, Pittsburgh, PA 15260*

<sup>7</sup> *SUNY, Stony Brook, NY 11794*

<sup>8</sup> *University of São Paulo, Brazil*

<sup>9</sup> *Wayne State University, Detroit, MI 48202*

(July 4, 2000)

New data on  $\Lambda$  production in Au+Au collisions at 11.5 A GeV/c are presented. The measurements cover the rapidity range from  $y=2.0$  to 3.5 and transverse momenta from  $p_t=0.15$  GeV/c to 1.5 GeV/c. The rapidity distributions, transverse momentum spectra, and azimuthal distributions are presented for different centralities of the collision. A strong positive directed flow at forward rapidity is observed for semicentral collisions. The measured spectra, yields and directed flow are compared with the predictions of RQMD v2.3 model.

## I. INTRODUCTION

Strangeness production in heavy-ion collisions when compared to proton-proton collisions is potentially a sensitive probe of collective energy deposition and therefore of heavy ion reaction mechanisms in general. Its study may provide insight into the properties of hot and dense nuclear matter [1]. Indeed, enhanced strangeness production has been observed at AGS and SPS energies [2,3].

Experimental measurements indicate that high baryon density is reached in central heavy-ion collisions at both AGS [4,5] and SPS [6]. Via comparisons with models that reproduce the experimental data, it has been concluded that one reaches baryon densities of up to 10 times normal nuclear matter density and energy densities of the order of 2 GeV/fm<sup>3</sup> in the center of the fireball [7]. These values are well into the range where, based on lattice QCD calculations, one expects a baryon-rich deconfined phase. The realization [8,9] that fireballs with saturated strangeness cannot be produced in purely hadronic scenario has lent strong support to the interpretation that a deconfined (at least partly) phase has been found in central ultrarelativistic nuclear collisions. Consequently it is of great importance to investigate further aspects of strangeness production, such as, e. g., flow effects.

The experimental and theoretical studies of collective flow of various types have been an important component of the investigation of relativistic heavy-ion collisions [10–13]. The experimental data on transverse collective flow phenomena at Bevalac and SIS energies (1–2A GeV) [10], AGS (4–11A GeV) [14–17] and SPS energies (150–200A GeV) [18–21], have led to a renewed intense theoretical interest in this topic [22–27]. It was pointed out that collective flow directly probes the equation of state of nuclear matter and can provide a useful information about the possible phase transition [23,25].

In order to obtain the information about the nuclear equation of state, systematic studies of freeze-out observables as a function of collision system size and bombarding energy are necessary [11–13]. These observables include strangeness and antibaryon production. Since the bulk of strangeness produced is carried by kaons, measurements of kaon spectra and their flow in heavy-ion collisions have been systematically carried out at different energies [10,28,29] and their in-medium properties have been investigated [30].

Experimental studies of  $\Lambda$  and  $\bar{\Lambda}$  production and flow are now available at SIS/GSI [31,32]

and at AGS energies [33–40]. At SIS energies it was found that the  $\Lambda$  mean field constructed on the basis of the quark model leads to a good description of the observed in-plane transverse flow of  $\Lambda$ 's [41]. Differences between the  $K^+$  and  $\Lambda$  flow due to their different mean field potential in dense matter have also been discussed [42]: while the  $\Lambda$  flow is basically similar to that of nucleons, the  $K^+$  flow almost disappears. Recently, directed flow of neutral strange particles in heavy-ion collisions at AGS has been investigated in a relativistic transport model (ART) [43], showing that the smaller  $\Lambda$  directed flow relative to the proton flow can be accounted for by a weaker mean-field potential as in the constituent quark model and from hypernuclei phenomenology. Therefore, a detailed study of the directed flow of strange particles in conjunction with other variables should help in understanding the relative importance of different reaction mechanisms.

In this paper we present new experimental results on  $\Lambda$  production obtained from the 1995 run of the E877 experiment. In section 2, we briefly describe the experimental setup. In section 3, the analysis steps for  $\Lambda$  identification are discussed. The experimental results, including the rapidity distributions, invariant mass spectra, and azimuthal distributions, and their comparison with RQMD v2.3 model are presented in section 4. Discussion and conclusion will be given in the last section.

## II. E877 APPARATUS

A schematic view of the E877 apparatus is shown in Fig. 1. For the 1995 run, the silicon beam vertex detectors (BVER's) were upgraded from single-sided silicon wafers with one-dimensional pitch of 50  $\mu\text{m}$  to double-sided wafers with a 200  $\mu\text{m}$  pitch in both the  $x$  and  $y$  directions (see Fig. 1). Using these detectors the position and angle of beam particles at the target were determined with an accuracy of 300  $\mu\text{m}$  in coordinates and 60  $\mu\text{rad}$  in angle. The centrality of the collision and reaction plane orientation were obtained from the transverse energy distribution measured in the target calorimeter (TCAL), and participant calorimeter (PCAL). Both calorimeters had  $2\pi$  azimuthal coverage and combined, provided nearly complete polar angle ( $\theta$ ) coverage: TCAL and PCAL covered the pseudorapidity regions  $-0.5 < \eta < 0.8$  and  $0.8 < \eta < 4.2$ , respectively, where  $\eta = -\ln[\tan(\theta/2)]$ . The centrality selection was quantified by the ratio  $\sigma_{top}/\sigma_{geom}$ , where  $\sigma_{top} = \int_{E_t}^{\infty} (d\sigma/dE_t') dE_t'$  and  $\sigma_{geom}$  is

the geometrical cross section of the colliding Au+Au nuclei. The analysis of anisotropic transverse collective flow requires the precise determination of the reaction plane which is defined by the impact parameter vector and the beam axis. The reaction plane orientation was determined event by event from the azimuthal anisotropy in the transverse energy distribution [45]. The reaction plane resolution was evaluated by studying the correlation between flow angles measured in different pseudorapidity intervals [44,45].

Charged particles emitted in the forward direction and passing through a collimator ( $-134 \text{ mrad} < \theta_{horizontal} < 16 \text{ mrad}$ ,  $-11 \text{ mrad} < \theta_{vertical} < 11 \text{ mrad}$ ) were analyzed in a high resolution magnetic spectrometer. The spectrometer acceptance covered mostly the forward rapidity region. The momentum of each particle was measured using two drift chambers, DC2 and DC3, whose pattern recognition capability was aided by four multi-wire proportional chambers (MWPC). The average momentum resolution was  $\Delta p/p \approx 3\%$  limited by multiple scattering. A time-of-flight hodoscope (TOFU) located directly behind the tracking chambers provided the time-of-flight with an average resolution of 85 ps [46]. Energy loss information from TOFU was used to determine the particle charge.

For the 1995 run, two identical highly segmented cathode pad detectors (VTX) were instrumented and installed between the PCAL/collimator and the spectrometer magnet (Fig. 2). They provided a precise measurement of the x-coordinate (bending plane coordinates) of the track before deflection in the magnetic field. This allowed to reconstruct the decay vertices of the particles such as  $\Lambda$  baryons and improve the signal-to-background ratio for identification of rare particles such as  $K^-$  and antiprotons. The active area of each pad chamber consisted of 10 rows of chevron shape pads with each row having 53 pads and one anode wire placed above each row. The position resolution along the x-direction was about  $300 \mu\text{m}$ , while the resolution in y-direction was determined by the wire spacing (5 mm). A detailed description of the design, implementation and performance of the vertex chambers can be found in [47].

### III. DATA ANALYSIS

In our data analysis  $\Lambda$ 's were identified by reconstructing  $(p, \pi^-)$  pairs from their characteristic  $V_0$  decay topology  $\Lambda \rightarrow p + \pi^-$ . Single tracks were first reconstructed by the standard

E877 tracking program “Quanah” [48] which assumed that particle originates from the target. The invariant mass of  $(p, \pi^-)$  pair was calculated using  $\Lambda$ -decay kinematic hypothesis only and was used for the  $\Lambda$  identification. To separate the  $\Lambda$ 's from a large combinatorial background of the directly produced  $p$  and  $\pi^-$ , we performed the following analysis steps.

From the information provided by the VTX detectors, which are not part of the standard E877 tracking program, we determined the track segments upstream of the spectrometer magnet for  $p$  and  $\pi^-$  and reconstructed the assumed decay vertex  $(V_x, V_y, V_z)$  of the pair by finding the crossing point of the  $p$  and  $\pi^-$  tracks. Since the tracking detectors had a better position resolution in the bend plane (x-z plane) of the spectrometer, only the values  $V_x$  and  $V_z$  were used for the elimination of the combinatorial background.

A set of conditions was applied to reduce the background. First, it was required that the z-position of the decay vertex was between 25 and 180 cm downstream of the target. The minimum value was limited by the VTX chambers resolution and the maximum value was limited by the geometric position of the first VTX chamber. This condition drastically reduced the large combinatorial background but also rejected about 28% of the true  $\Lambda$ 's in our acceptance. The proton and pion tracks were also required to point away from the interaction point in the target in the x-direction. We rejected the proton tracks which, after projecting back to the target, were less than 4 mm away from the x-coordinate of the interaction point. For pions we required the x-coordinate to be more than 14 mm away from the interaction. These cuts were very effective in rejecting pairs containing primary protons and pions but they also eliminated  $\Lambda$ 's whose decay products were emitted along the  $\Lambda$  momentum vector.

Besides the above selections, we also required that the upstream track segment determined by the VTX detectors and downstream track segment identified by the tracking program matched at the center of the spectrometer magnet. A  $3\sigma$  cut was applied on the difference in x-positions obtained from fitting the upstream and downstream track segments. The reconstructed momentum vector of the pair was also required to point back to the interaction point within 2.0 mm ( $3\sigma$  cut) in x-direction.

All described cuts were optimized using a Monte Carlo simulation [49]. After filtering by this set of conditions, the combinatorial background is dramatically reduced, so the  $\Lambda$  peak

is well identified in the invariant mass distribution. A further improvement was obtained by recalculating the proton and pion momenta using as origin the decay vertex position obtained from VTX detectors. This significantly improved the mass resolution of the  $\Lambda$  peak as well as the signal-to-background ratio (see Fig. 3). The remaining background under the  $\Lambda$  peak is mainly due to the accidental combination of proton and pion tracks passing our cuts.

In order to reconstruct the  $\Lambda$  spectra, the data need to be corrected for the spectrometer acceptance and the effects of the various conditions introduced in the analysis. The single track efficiency of the spectrometer downstream of the magnet was discussed in [50]. We studied the efficiency of the upstream VTX detectors by looking into the proton yield ratio with and without the VTX cut. The obtained efficiency of VTX detectors was about 85% for single tracks in the sensitive area of the detectors.

The acceptance corrections for  $\Lambda$  distributions were calculated using a detailed Monte-Carlo simulation. Au+Au events were generated using the RQMD v2.3 event generator [51,52]. The acceptance corrections on the final data sample were calculated as a function of rapidity  $y$  and transverse momentum  $p_t$  by propagating the generated particles through the E877 apparatus. All the known effects of the spectrometer geometry, detector resolutions, kinematics and cuts were included into the calculation. The acceptance for  $\Lambda$ -hyperons is of the order  $10^{-3}$  for beam rapidity region  $3.0 < y < 3.2$ , where there is relatively high reconstruction efficiency, and  $10^{-4}$  or less for rapidity range  $2.2 < y < 2.5$ . The uncertainties in the estimation of the acceptance corrections, efficiency of the VTX detectors, and background subtraction, result in an overall systematic uncertainty of the order of 15% in the estimated  $\Lambda$  yield. After the background subtraction, we identified 2644  $\Lambda$ 's from 32 millions events with centrality  $\sigma_{top}/\sigma_{geom} < 10\%$ .

Fig. 4 shows the  $\Lambda$  acceptance in the  $(p_t, y)$  phase space. The E877 spectrometer covers a rapidity range of  $2.2 < y < 3.4$  and transverse momenta  $p_t > 0.15$  GeV/c.  $\Lambda$ 's at low  $p_t$  were not reconstructed due to the dead zones in the VTX detectors near the beam axis.

#### IV. RESULTS

## A. Lambda Yield and Spectra

The data were divided into constant  $p_t$  bins of 100 MeV and rapidity bins of 0.3 unit width from  $y = 2.2$  to  $y = 3.4$ . The lambda yield was obtained from the invariant mass distributions in each  $(y, p_t)$  bin after corrections for acceptance, efficiency and background subtraction as described in section III. In Fig. 5,  $\Lambda$  transverse mass spectra are presented for the most central collisions ( $\sigma_{\text{top}}/\sigma_{\text{geom}} < 4\%$ ) and for semicentral collisions ( $4\% < \sigma_{\text{top}}/\sigma_{\text{geom}} < 10\%$ ). The error bars include statistical errors and the errors from the background subtraction procedure. The range in  $m_t$  reflects the acceptance of the spectrometer in the different rapidity bins. The solid lines represent the best fits to the spectra using Boltzmann distribution :

$$\frac{1}{m_t^2} \cdot \frac{d^2N}{dm_t dy} = \frac{N_B}{m_\Lambda} \cdot \exp\left(-\frac{m_t - m_\Lambda}{T_B(y)}\right) \quad (1)$$

where  $T_B(y)$  is the inverse slope of the spectrum. The experimental  $m_t$  spectra are in good agreement with this exponential shape.

The Relativistic Quantum Molecular Dynamics (RQMD) model [51] has been widely used in describing relativistic heavy-ion collisions. It combines the classical propagation of all hadrons with string and resonance excitations in the primary collisions of nucleons from the target and projectile. Overlapping color strings may fuse into so-called ropes. Subsequently, the fragmentation products from rope, string and resonance decays interact with each other and with the original nucleons, mostly via binary collisions. These interactions drive the system towards equilibrium [52] and are responsible for the development of collective flow, even in the pre-equilibrium stage. If baryons are surrounded by other baryons they acquire effective masses. The effective masses are generated by introducing Lorentz-invariant quasi-potentials into the mass-shell constraints for the momenta, which simulates the effect of *mean field* [24]. There are no potential-type interactions in the so-called *cascade mode* of RQMD.

A comparison with RQMD v2.3 model run in *cascade* (dashed histograms) and *mean field* modes (dotted histograms) is also presented in Fig. 5. We can see that the conventional transport hadronic model reproduces the data relatively well in magnitude and shape over the measured rapidity and centrality intervals. We note, however, especially in the forward

rapidity region, significant (up to a factor of 2) differences between the cascade and mean-field modes of RQMD.

The derived lambda inverse slopes  $T_B(y)$  are shown in Fig. 6. The data for  $\Lambda$ -hyperons are also compared to the slopes obtained from the proton spectra analysis [50]. Error bars on the fit parameters are statistical only. Except for the first data point for which the systematic error is large due to the limited range of the measured  $m_t$  spectra, the inverse slope parameters extracted from the  $\Lambda$  spectra are, for both centrality bins, similar to those of the protons. This is consistent with protons and  $\Lambda$ 's having a similar collective flow which is superimposed on the thermal motion at freeze-out.

By integrating the transverse mass spectra where data are available and using the results from the Boltzmann fits to extrapolate to infinity and to  $p_t = 0$  we obtain the  $\Lambda$  rapidity distributions shown in Fig. 7 for the two centrality intervals. The data are compared with the RQMD v2.3 predictions. The data are, within the systematic errors, in good agreement with the model predictions. In the experimentally covered rapidity range ( $2.2 < y < 3.4$ ), cascade and mean field calculations show a similar  $\Lambda$ -yield. A discrepancy between the two predictions of RQMD v2.3 appears in the midrapidity region, which is not covered by our experiment. A similar effect in RQMD calculations of proton yield has been recently noted [53].

Fig. 7 also includes a comparison with the results from the E891 experiment [38] at AGS, which covered a similar rapidity range. The E891 collaboration reported a yield which is roughly 20 % higher than ours. Such a difference is at the limit of the systematic errors of both experiments.

## B. Lambda Directed Flow

At lower beam energies ( $< 2$  A·GeV), theoretical studies show that directed flow of lambda hyperons is very sensitive to the  $\Lambda$  potential in dense nuclear matter formed in heavy-ion collisions [58]. The calculations also show that, at this energy, the primordial lambda hyperons have a weak flow as compared to nucleons. However, final-state interactions, and especially the propagation in mean-field potentials, enhance the lambda flow in the direction of nucleons and bring the theoretical results in good agreement with the experimental data



from the FOPI [31] and EOS [32] collaborations.

For an emission dominated by directed flow, the azimuthal distribution can be parameterized by

$$\frac{1}{N_0} \frac{dN}{d\varphi} = 1 + 2v_1 \cos \varphi \quad (2)$$

where  $\varphi = \phi - \psi_r$ ,  $\phi$  is the azimuthal angle of the particle in the lab frame, and  $\psi_r$  is the reaction plane angle. The parameter  $v_1$  quantifies directed flow of particles parallel ( $v_1 > 0$ ) or antiparallel ( $v_1 < 0$ ) to the impact parameter vector.

We studied the azimuthal angular distribution with respect to the reaction plane to extract the average directed flow parameter  $v_1$  estimated in the experimental  $p_t$ -acceptance for different rapidity and centrality windows. We divided the azimuthal angle range from  $-180^\circ$  to  $180^\circ$  into six equal bins. In order to obtain the azimuthal angular distribution of  $\Lambda$ 's, the  $\Lambda$  yield was extracted from the invariant mass distribution in each azimuthal angle bin after background subtraction. The obtained semi-inclusive azimuthal angular distributions of  $\Lambda$ 's with respect to the reaction plane are presented in Fig. 8. In the most central bin ( $< 4\% \sigma_{geom}$ ), as can be expected, there is no/or very little anisotropy in the azimuthal distributions. But in the semi-central bin ( $4 - 10\% \sigma_{geom}$ ), the azimuthal distributions exhibit a directed flow signal which becomes significant for the forward rapidity window.

We also studied the differential flow ( $p_t$  dependence of  $v_1$ ) as a function of rapidity and centrality using the Fourier expansion method which was previously used for the analysis of proton and pion directed flow [54]. The results are presented in Fig. 9. In agreement with the inclusive azimuthal angular distributions within statistical errors data show no directed flow for central collisions ( $< 4\% \sigma_{geom}$ ). A positive and statistically significant signal is observed for the semi-central collisions and forward rapidities ( $2.8 < y < 3.4$ ).

Since nucleons are the major carriers of flow signal and directed flow of protons has been well studied [15,16], it provides a good reference for comparison with flow of other particles. The predictions of RQMD model v2.3 for proton and  $\Lambda$  directed flow in Au+Au collisions are shown in Fig. 10. As it has recently been shown, RQMD well describes the amplitude of the experimentally measured proton flow if the effects of mean-field are included. However, RQMD predictions for differential flow differ significantly from the data, both for cascade

and mean field modes [15,16].

In general, RQMD predicts that  $\Lambda$  flow should be very similar to proton flow. Both cascade and mean-field calculations predict that flow of  $\Lambda$ 's is very small at mid-rapidity and that it becomes larger and comparable with the proton flow at  $y > 2.5$ . This is the region well covered by our experimental measurements. A close inspection of the mid-rapidity region in Fig. 10 reveals that a very small anti-flow is predicted by the mean-field calculations with a transition from negative to positive flow occurring around  $y = 2.4$ .

The comparison between the measured data and RQMD v2.3 predictions are presented in Fig. 11. Although the interpretation of the  $v_1(p_t)$ -dependence is limited due to low statistics, one can conclude that the measured  $p_t$  dependence of lambda directed flow is consistent with that predicted by the model. The cascade calculations give a somewhat better description of the trend exhibited by the data.

At lower beam energies (around 2 A·GeV), theoretical calculations from the relativistic transport models indicate that mean-field potentials play a major role in development of  $K^+$  and  $\Lambda$  flows [55]. Without any final-state interaction, both  $K^+$  and  $\Lambda$  flow in the same direction as nucleons, but with much smaller flow amplitudes. The inclusion of rescattering with the dense matter just enhances the flow of  $K^+$  and  $\Lambda$  in the direction of nucleons, as a result of thermalization effects. However, the propagation of  $K^+$  and  $\Lambda$  in their mean-field potentials leads to significantly different flow patterns for  $K^+$  and  $\Lambda$ . Kaons are pushed away from nucleons by their repulsive potential while lambda hyperons are pulled towards nucleons by their attractive potential. This leads to a predicted small anti-flow of kaons with respect to nucleons, and to a flow of lambda hyperons of amplitude very close to the flow of nucleons.

Fig. 12 shows the comparison of  $K^+$  directed flow data [56,57] with the RQMD v2.3 predictions. Similar to results presented here, the cascade calculations give a better description of the data. Since  $\Lambda$  production is mainly associated with kaons in hadronic scenario, whether  $K^+$  and  $\Lambda$  medium effects persist at the AGS or even higher energies is still an open question.

## V. SUMMARY AND CONCLUSION

The lambda spectra have been measured as a function of transverse mass and rapidity for different collision centralities. The spectra are well described by an exponential with inverse slopes decreasing with increasing rapidity. The derived lambda inverse slopes are similar to those obtained from the proton  $m_t$  spectra. This is consistent with the picture of  $\Lambda$ 's originating from a fireball in local thermal equilibrium.

We have observed, for the first time at AGS, a significant positive directed flow of lambda hyperons at forward rapidities ( $2.8 < y < 3.4$ ) in semi-central Au+Au collisions. The average flow amplitude for lambda hyperons is comparable with that for protons for the same acceptance region. This result is consistent with the measurements performed at lower energies ( $< 2A \cdot \text{GeV}$ ), and suggests that lambda flow follows the flow of nucleons.

The measurements have been compared to the predictions of RQMD model (v2.3) run in *cascade* and in *mean-field* modes. In the covered rapidity range, the model describes the spectra rather well. The measured differential flow ( $v_1(p_t)$ ) is comparable to the model predictions, with a better description provided by the cascade calculations.

## ACKNOWLEDGMENTS

We thank the AGS staff, W. McGahern and Dr. H. Brown for excellent support and acknowledge the help of R. Hutter in all technical matters. Financial support from the US DoE, the NSF, the Canadian NSERC, and CNPq Brazil is gratefully acknowledged.

- 
- [1] P. Koch, B. Müller and J. Rafelski, Phys. Rep. **142** (1986).
  - [2] L. Ahle et al., Phys. Lett. **B476**, 1 (2000).
  - [3] F. Antinori et al., Nucl. Phys. **A661**, 476c (1999).
  - [4] J. Barrette et al. (E877 Collaboration), Phys. Rev. C **51**, 3309 (1995).
  - [5] L. Ahle et al. (E802 Collaboration), Phys. Rev. C **57**, R466 (1998).

- [6] H. Appelshäuser et al. (NA49 Collaboration), Phys. Rev. Lett. **82**, 2471 (1999).
- [7] J. Stachel, Nucl. Phys. **A654**, 119c (1999).
- [8] P. Braun Munzinger and J. Stachel, Nucl. Phys. **A606**, 320 (1996).
- [9] U. Heinz, Nucl. Phys. **A661**, 140c (1999) ; R. Stock, Phys. Lett. **B456**, 277 (1999).
- [10] W. Reisdorf and H. G. Ritter, Annu. Rev. Nucl. Part. Sci. **47**, 663 (1998).
- [11] S. A. Bass, M. Gyulassy, H. Stöcker and W. Greiner, J. Phys. G. **25**, R1 (1999).
- [12] F. Wang, Heavy ion physics from Bevalac to RHIC (Edited by R. Seto, Singapore, World Scientific, 1999) pp195-204.
- [13] W. Cassing and E. L. Bratkovskaya, Phys. Rep. **308**, 67 (1999).
- [14] J. Barrette et al. (E877 Collaboration), Phys. Rev. Lett. **73**, 2532 (1994).
- [15] J. Barrette et al. (E877 Collaboration), Phys. Rev. C **55**, 1420 (1997).
- [16] J. Barrette et al. (E877 Collaboration), Phys. Rev. C **56**, 3254 (1997).
- [17] C. Pinkenburg et al. (E895 Collaboration), Phys. Rev. Lett. **83**, 1295 (1999).
- [18] T. Wienold et al. (NA49 Collaboration), Nucl. Phys. **A610**, 76c (1996).
- [19] I. Bearden et al. (NA44 Collaboration), Phys. Rev. Lett. **78**, 2080 (1997).
- [20] H. Appelshäuser et al. (NA49 Collaboration), Phys. Rev. Lett. **80**, 4136 (1998).
- [21] F. Ceretto et al., Nucl. Phys. **A638**, 467c (1998).
- [22] J. Y. Ollitrault, Nucl. Phys. **A638**, 195c (1998).
- [23] D. Rischke and M. Gyulassy, Nucl. Phys. **A597**, 701 (1996).
- [24] H. Sorge, Phys. Rev. Lett. **78**, 2309 (1997).
- [25] H. Sorge, Phys. Rev. Lett. **82**, 2048 (1999).
- [26] U. Heinz, J. Phys. **G25**, 263 (1999).
- [27] H. Heiselberg and A. M. Levy, Phys. Rev. C **59**, 2716 (1999).

- [28] P. Senger and H. Ströbele, J. Phys. **G25**, R59 (1999).
- [29] C. A. Ogilvie (E866 and E917 Collaboration), J. Phys. **G25**, 159 (1999).
- [30] G. Q. Li and G. E. Brown, Phys. Rev. C **58**, 1698 (1998).
- [31] J. L. Ritman et al. (FOPI Collaboration), Z. Phys. **A352**, 355 (1995).
- [32] M. Justice et al. (EOS Collaboration), Phys. Lett. **B440**, 12 (1998)
- [33] S. E. Eiseman et al., Phys. Lett. **B297**, 44 (1992) ; idem Phys. Lett. **B325**, 322 (1994).
- [34] S. Ahmad et al. (E891 Collaboration), Phys. Lett. **B382**, 35 (1996).
- [35] Y. Wu et al. (E859 Collaboration), Proceedings of Heavy Ion Physics at the AGS, HIPAGS'96, 22-24 August, 1996 (edited by C. A. Pruneau, G. Welke, R. Bellwied, S. J. Bennett, J. R. Hall and W. K. Wilson), WSU-NP-96-16, 37 (1996)
- [36] X. Yang et al. (E910 Collaboration), Proceedings of Heavy Ion Physics at the AGS, HIPAGS'96, 22-24 August, 1996 (edited by C. A. Pruneau, G. Welke, R. Bellwied, S. J. Bennett, J. R. Hall and W. K. Wilson), WSU-NP-96-16, 75 (1996)
- [37] D. Best et al. (E895 Collaboration), J. Phys. **G23**, 1873 (1997).
- [38] S. Ahmad, B. E. Bonner, S. V. Efremov, G. S. Mutchler, E. D. Platner, H. W. Themann, Nucl. Phys. **A636**, 507 (1998).
- [39] W. C. Chang et al. (E917 Collaboration), Proceedings of 15th Winter Workshop on Nuclear Dynamics, Park City, UT, 9-16 January, 1999, nucl-ex/9904010.
- [40] J. M. Alexander et al. (E895 Collaboration), J. Phys. **G25**, 255 (1999).
- [41] Z. S. Wang, A. Faessler, C. Fuchs, T. G. Boelting, Nucl. Phys. **A645**, 177 (1999).
- [42] G. Q. Li and G. E. Brown, Nucl. Phys. **A636**, 487 (1998).
- [43] Bin Zhang, C. M. Ko, Bao-An Li and A. T. Sustich, Phys. Rev. Lett. **83** 2534 (1999)
- [44] S. Voloshin and Y. Zhang, Z. Physik **C70**, 665 (1996).
- [45] Y. Dai, Ph. D thesis, McGill University, (1999).

- [46] R. Lacasse et al., Nucl. Instr. Meth in Phys. Res. **A408**, 408 (1998)
- [47] R. Bersch, M. Sc. Thesis, SUNY at Stony Brook, (1995).
- [48] J. Barrette et al. (E877 Collaboration), Phys. Rev. C **50**, 3047 (1994).
- [49] Y.J. Qi, Ph. D thesis, McGill University, (1999).
- [50] J. Barrette et al. (E877 Collaboration), Phys. Rev. C **71**, 036007 (2000)
- [51] H. Sorge, Phys. Rev. C **52**, 3291 (1995).
- [52] H. Sorge, Phys. Lett. **B373**, 16 (1996).
- [53] B. B. Back et al. (E917 Collaboration), Proceedings of 15th Winter Workshop on Nuclear dynamics, Park City, UT, 9-16 January 1999, nucl-ex/9904006
- [54] W.C. Chang, Ph. D thesis, SUNY at Stony Brook, (1997).
- [55] Z. S. Wang et al., Nucl. Phys. **A645**, 177 (1999).
- [56] K. Filimonov et al. (E877 Collaboration), Nucl. Phys. **A661**, 198c (1999).
- [57] J. Barrette et al. (E877 Collaboration), Nucl. Phys. **A661**, 379c (1999).
- [58] Bao-An Li and K. M. Ko, Phys. Rev. C **58**, R1382 (1998).

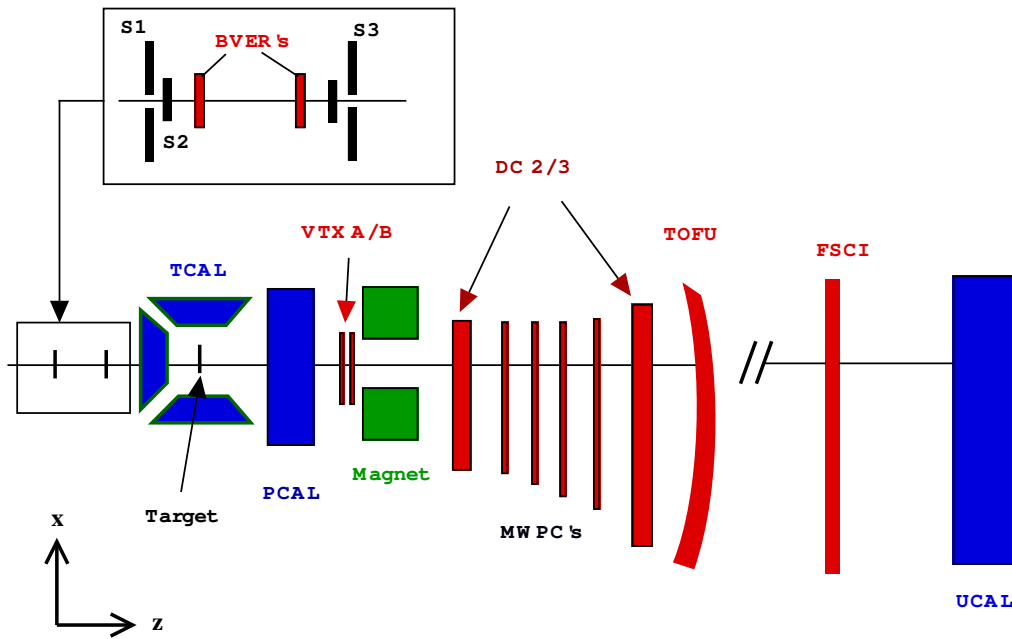


FIG. 1. Schematic view of the E877 experimental setup for the 1995 run. Au beam is incident from the left.

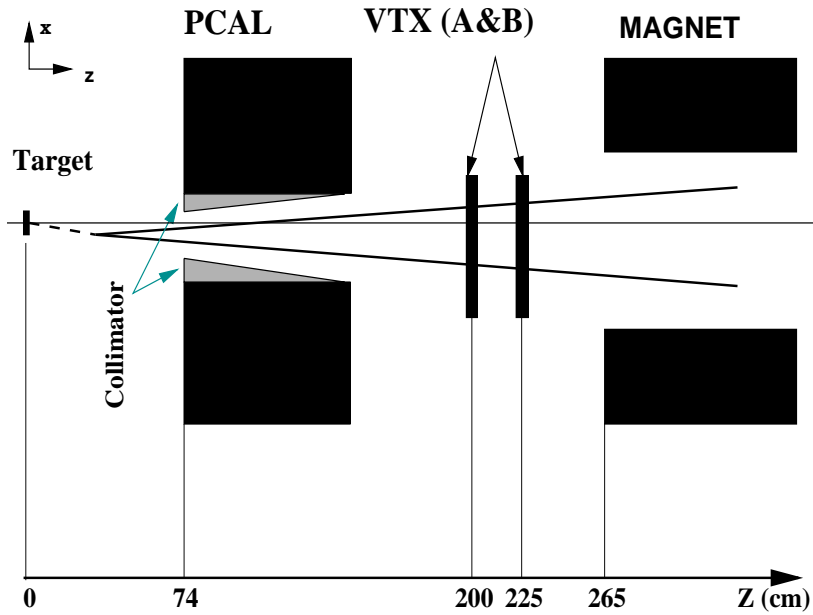


FIG. 2. Schematic layout of upstream detectors of the spectrometer.

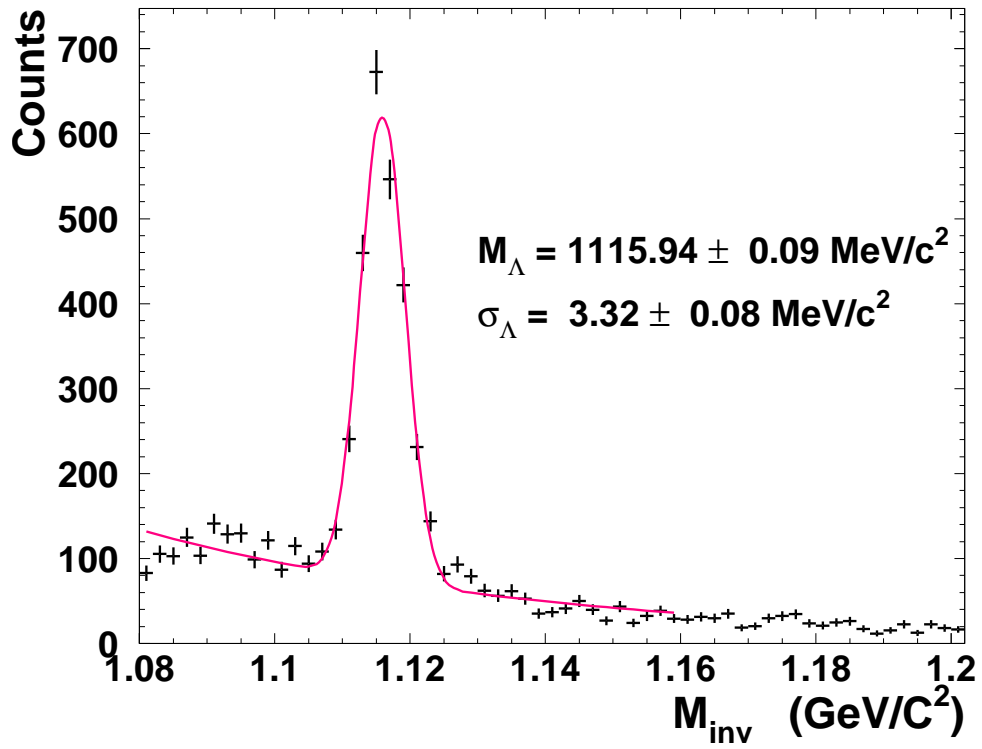


FIG. 3. Invariant mass distribution of  $(p, \pi^-)$  pairs.



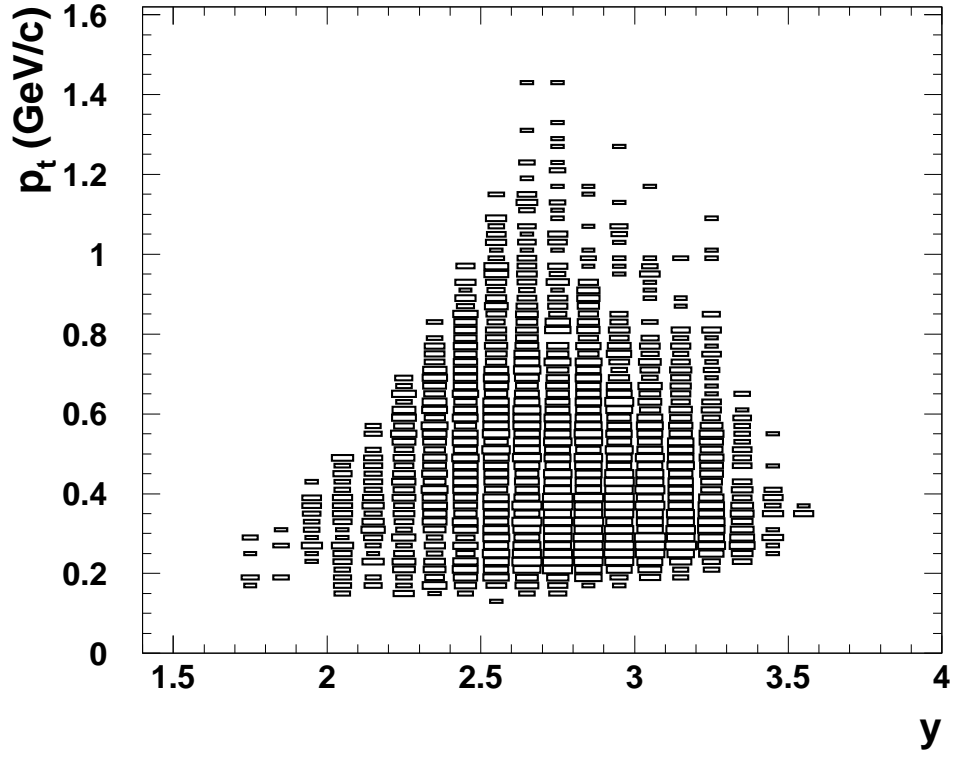


FIG. 4. The measured range for  $\Lambda$ 's in phase space after the applied cuts.

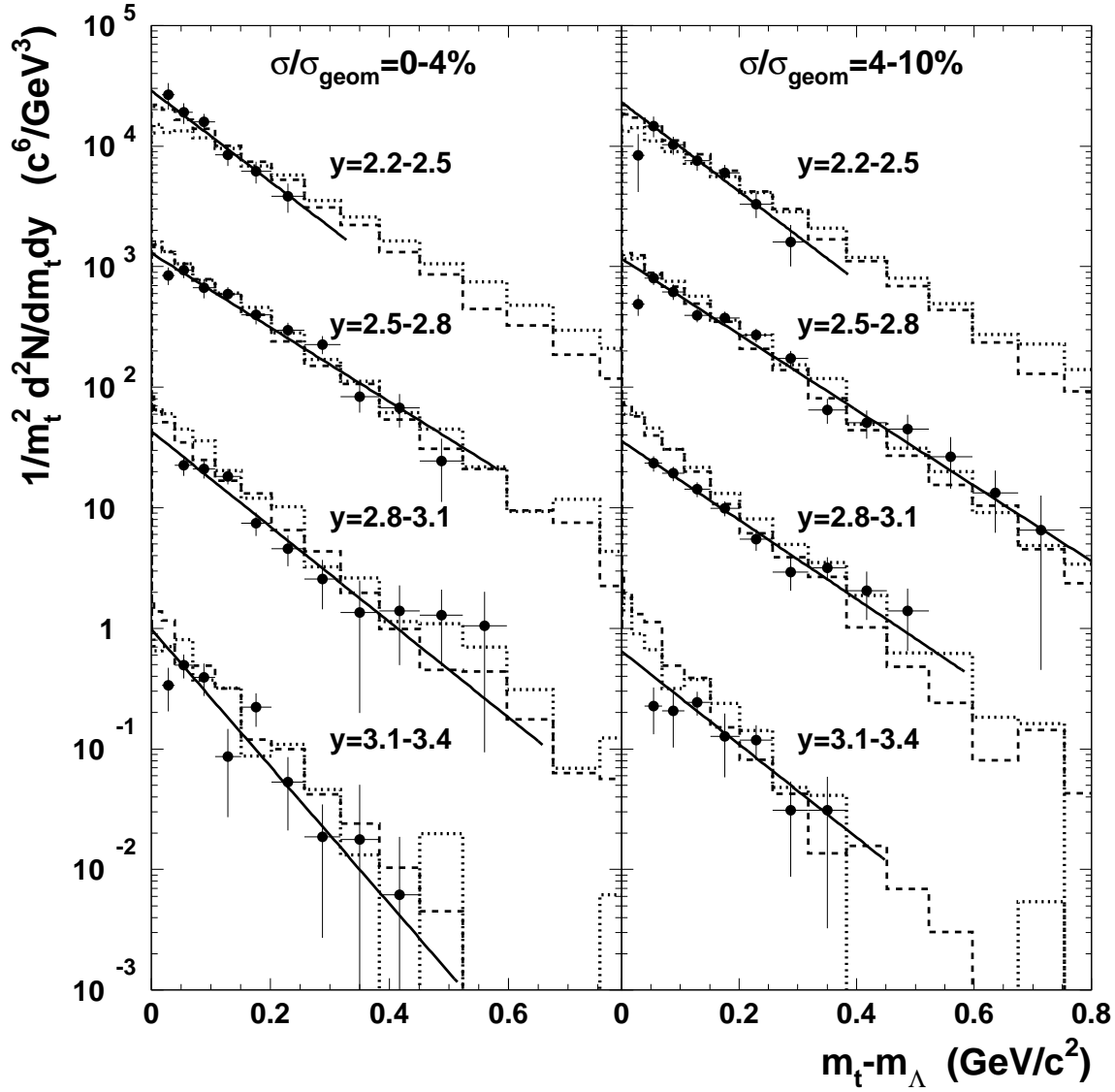


FIG. 5. Measured  $\Lambda$  transverse mass spectra for the most central ( $0 - 4\% \sigma_{geom}$ -left side) and semi-central ( $4 - 10\% \sigma_{geom}$  - right side) Au+Au collisions. Beginning with rapidity bin  $y=3.1-3.4$  spectra have been multiplied by successive factor of 10. The solid lines are the exponential Boltzmann fits to the data. The dashed lines and dotted lines are the predictions of RQMD v2.3 model run in *cascade* and *mean-field* modes, respectively.

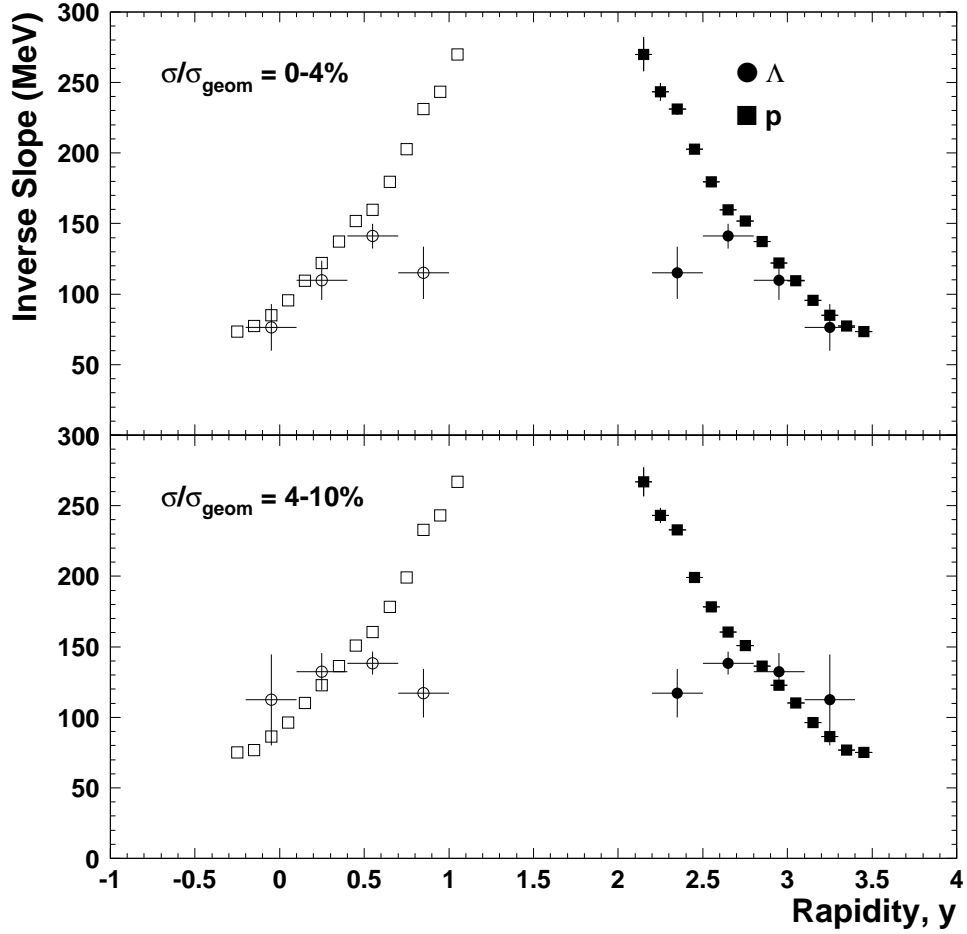


FIG. 6. The inverse slope parameters as a function of rapidity for central ( $0 - 4\% \sigma_{geom}$ -upper pannel) and semi-central ( $4 - 10\% \sigma_{geom}$  - lower pannel) Au+Au collisions. The data are represented by solid symbols and reflected about mid-rapidity (open symbols). The proton data are extracted from the 1995 data samples.

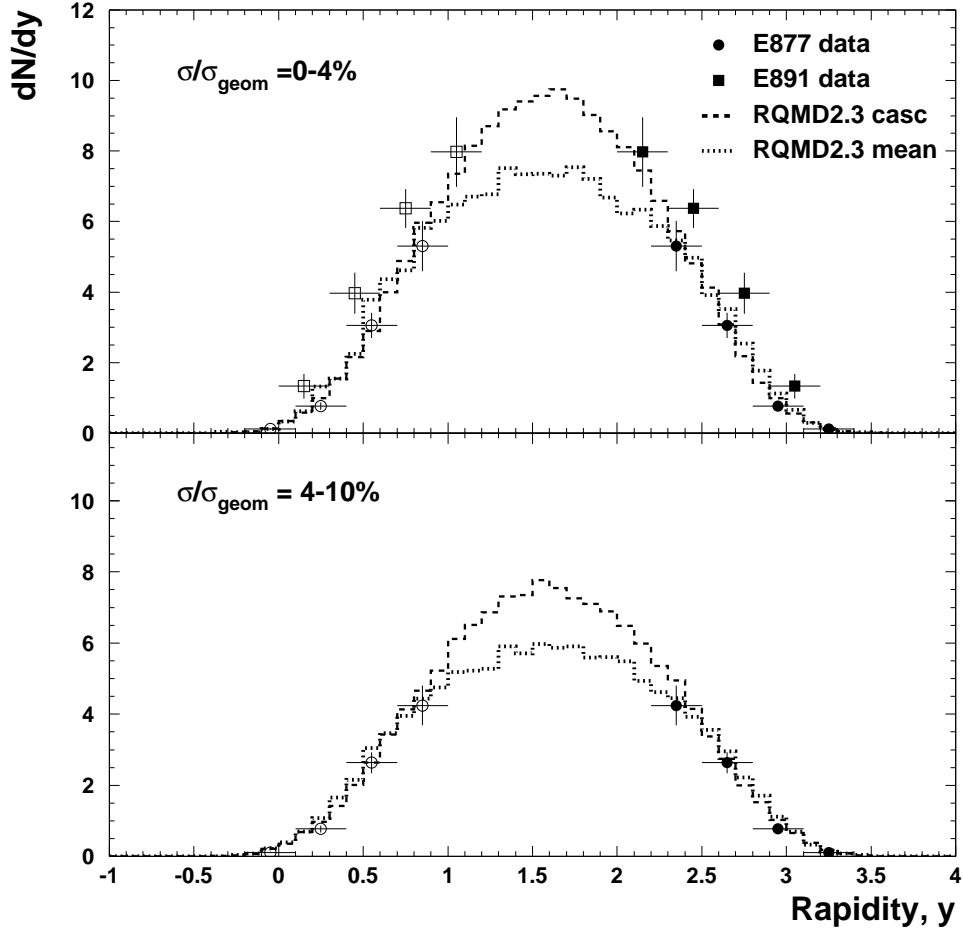


FIG. 7. Lambda rapidity distribution in the most central Au+Au collisions ( $0 - 4\% \sigma_{geom}$ -upper panel) and semi-central ( $4 - 10\% \sigma_{geom}$  - lower panel) Au+Au collisions. The data are represented by solid symbols and reflected about mid-rapidity (open symbols). The histograms correspond to RQMD v2.3 predictions.

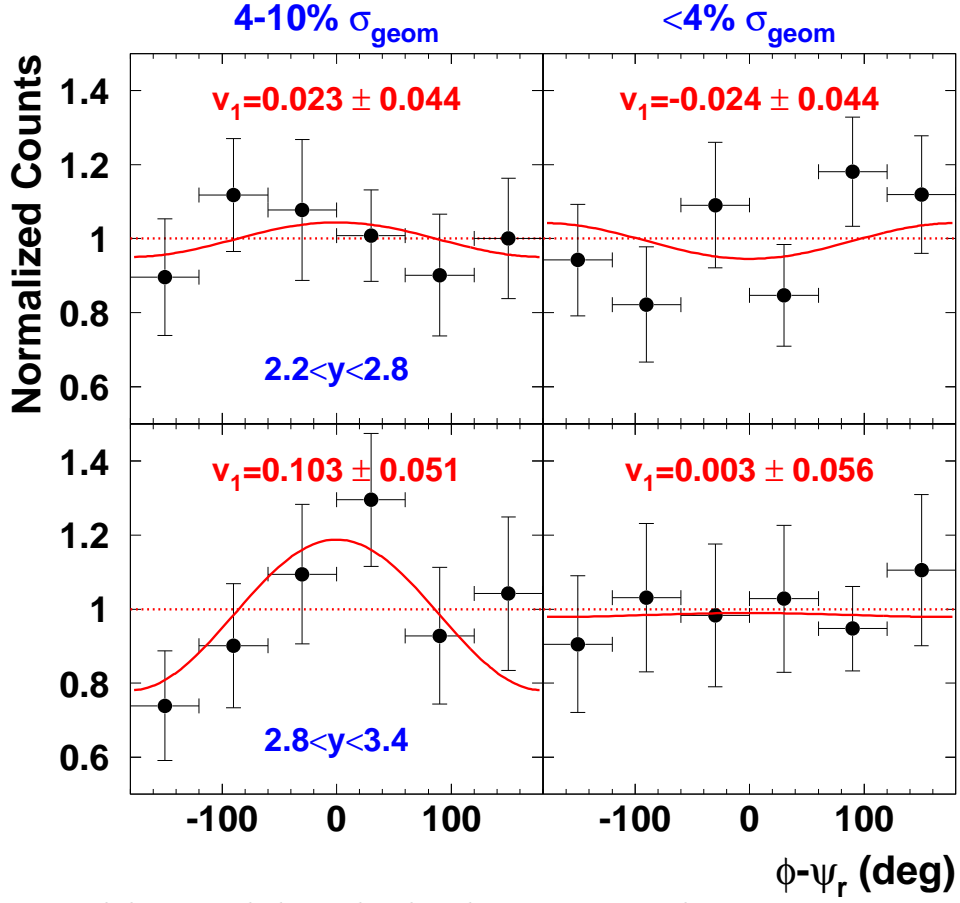


FIG. 8. Lambda azimuthal angular distributions measured in transverse momentum range  $0.15 < p_t < 1.5$  GeV/c for different rapidity and centrality bins. The distributions are normalized to unity. The solid lines are the fits using Eq. 2. The obtained values of  $v_1$  are uncorrected for the reaction plane resolution.

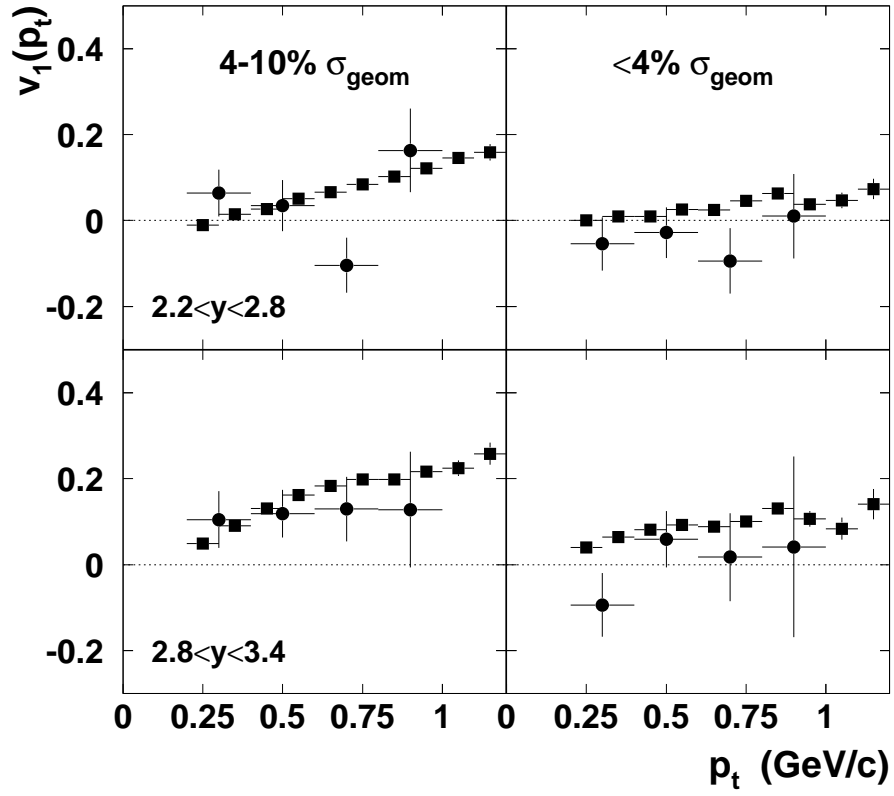


FIG. 9. Comparison of  $v_1(p_t)$  data between  $\Lambda$ 's (solid circles) and protons (solid squares).

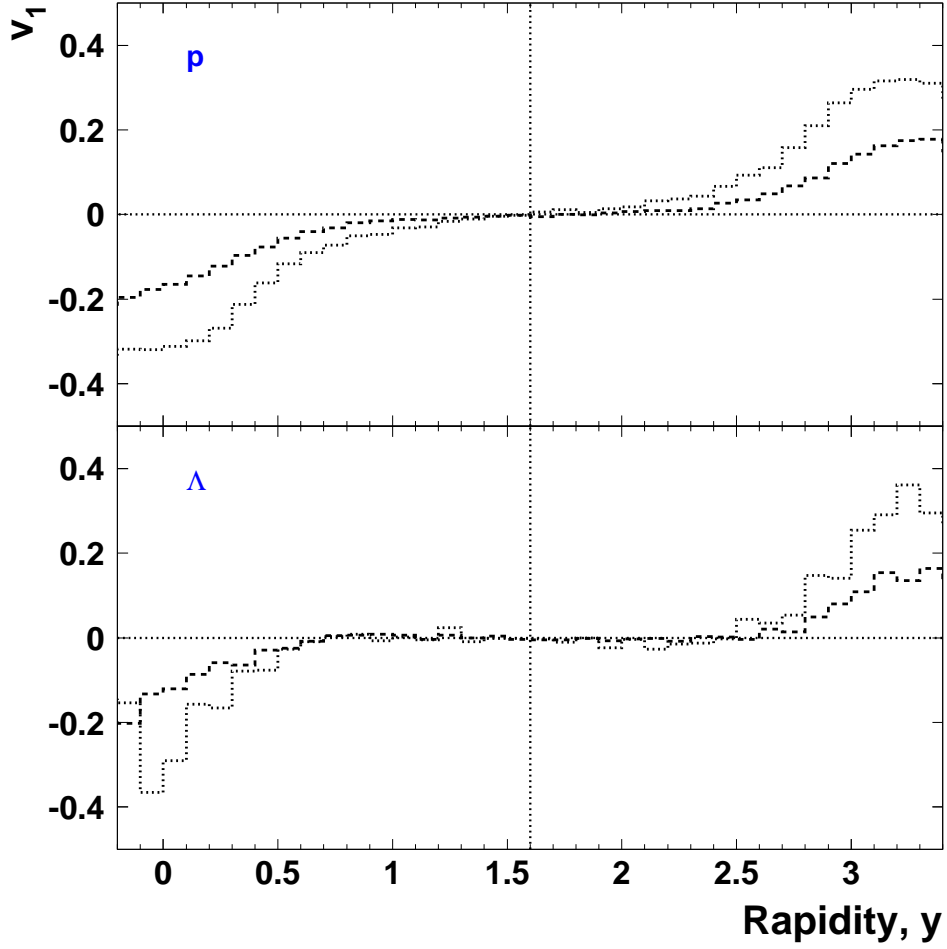


FIG. 10. Proton and lambda directed flows in Au+Au collisions ( $b < 10$  fm) at 11.5 A·GeV/c as a function of rapidity predicted by the RQMD model (v2.3) run in *cascade* mode (dashed histograms) and *mean-field* mode (dotted histograms).

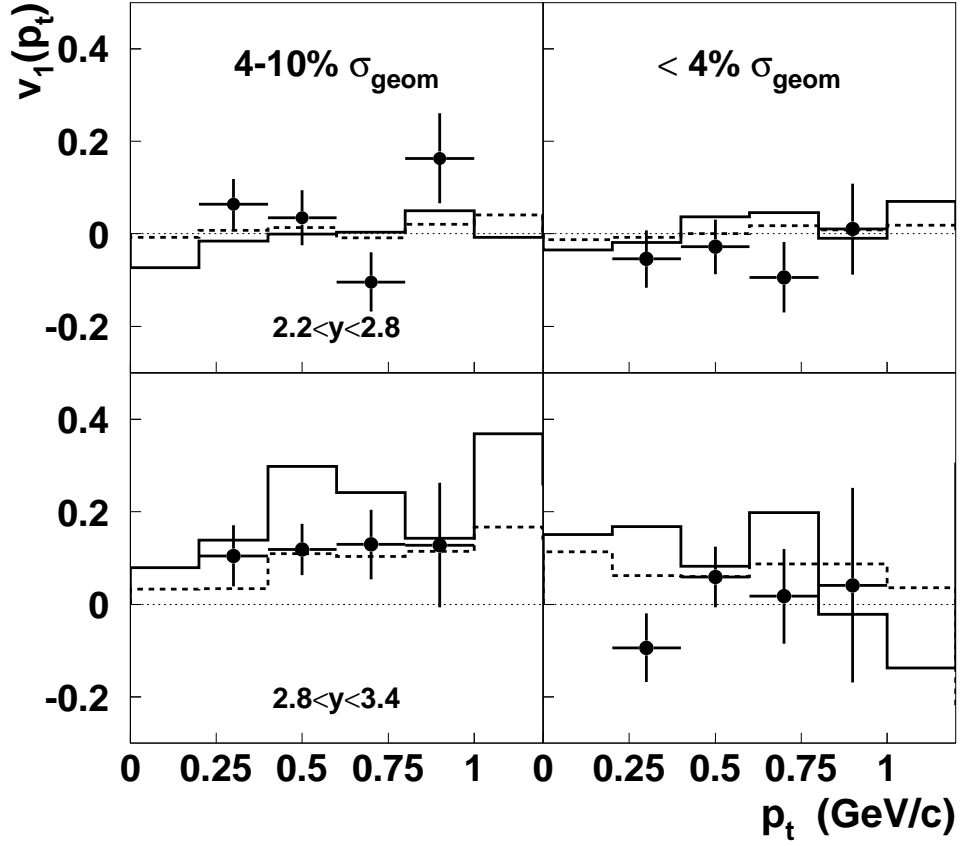


FIG. 11. Comparison of  $\Lambda$  flow data (solid circles) with the predictions of the RQMD v2.3 model, run in *cascade* (dashed histograms) and *mean-field* (full histograms) modes.



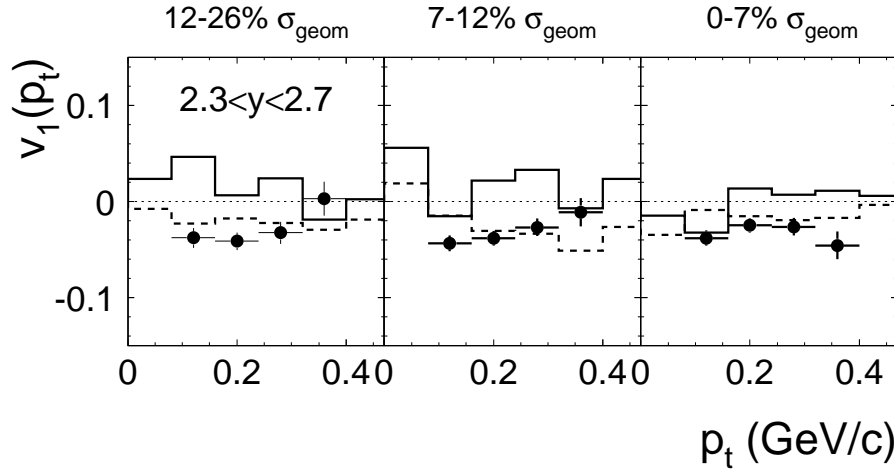


FIG. 12. Comparison of  $K^+$  flow data with the predictions of the RQMD v2.3 model. The histograms are the predictions of the RQMD model run in *cascade* (dashed histograms) and *mean-field* (full histograms) modes. The figure is taken from [57].